Analysis of the fragmentation function based on ATLAS data on proton-proton collisions at $\sqrt{s} = 7$ TeV

Elias Barba Moral

UNIVERSITY OF JYVÄSKYLÄ

Supervisors: Sami Räsänen, Dong Jo Kim

November 3, 2016

Preface

I want to thank the achievement of this work, firstly and mostly to the One I believe the Creator of everything, God, who gave the humans the entertaining job of figuring out what the world is made of. Next I want to thank my supervisors: Sami Räsänen, for leading me in all the steps of this work, being patient and kind with me; and Dong Jo Kim, who helped me on going through every step of this analysis including guiding most of the codes used in the analysis. To Jan Rak, leader of the ALICE group here in Jyväskylä, for trying to spread his passion for physics and suggesting the topic of this thesis. To Kari Eskola, who introduced me to particle physics and also supervised my Bachelor thesis and several courses. To all the classmates who have helped me through this two years. To the University of Jyväskylä, and specifically the Physics department for holding this masters program and giving funding for these years. Finally to all my family and friends who have cheered me from the distance.

Abstract

In high energy particle physics, the collision of two protons leads to quantum interactions through the strong force. This interactions produce highly energetic scattered particles that start to produce more particles forming collimated cones of particles, called jets. The phenomena that produces these jets from the scattered particles is called hadronization, and is explained using the fragmentation function.

In this work, the fragmentation functions from with the PYTHIA Monte Carlo event generator and the data from the ATLAS experiment in various jet energy ranges and they were used to study a cascade model proposed by Richard Feymann and Richard Field.

I found that PYTHIA is able to reproduce the ATLAS data with reasonable precision. The model results are presented using two different kinds of data: one being the same as used by ATLAS, and another with higher granularity data. The Feynman model is able to describe the data within ranges of 20% for most of the jet energy ranges available. It is remarkable how the results obtained by applying the model to the ATLAS data agree with the results of the model with the PYTHIA simulation.

Contents

1 Introduction

One of the main known constituents of the universe is the matter. The most of the matter we observe is made of atoms, which are made of protons and neutrons in a nucleus, and electrons orbiting around it. Protons, and hadrons in general, are made of quarks. In the Standard Model of particle physics, quarks are elementary particles. Quarks interact with each other mainly through the called strong force, and the gauge bosons (particles that mediate the interaction) are called gluons. This force hold together the quarks in the hadrons. Quarks and gluons are referred generally as partons.

Gell-Man postulated the existence of gluons in 1961 [1]. Gluons were confirmed experimentally by the TASSO Collaboration in DESY in 1979 [2]. Zweig [3] and Gell-Man [4] postulated independently the quarks in 1964. Initially only three quark flavors were proposed: up, down and strange. Within one year the charm quark was also postulated by Bjorken [5]. Finally in 1973 the remaining two of the known flavours, bottom and top, were added into the Standard Model [6]. The experimental evidence for the first quarks proposed came through the Stanford Linear Accelerator Center (SLAC) experiment in 1968 [7, 8], and the other flavours were confirmed later: charm quark [9], bottom quark [10] and top quark [11].

The charge that mediates the strong force (as electric charge mediates the electromagnetic force) is the color charge, and thus this field is called Quantum Chromodynamics (QCD). This was firstly described shortly after the quark postulation by Greenberg [12]. Each quark can exist with one of the different color states, called red, green or blue; but when they combine to form hadrons, those must have zero color charge. The fact that is only possible to observe isolated free particles with zero color charge is known as the color confinement property. Nevertheless gluons have 8 possible color states [13]. As gluons have a color charge, they interact among themselves and QCD has three and four gluon interaction vertices [14]. This is one the main difference to QED, where photons do not

interact [1]. Mathematically the difference comes from non-abelian nature of QCD [16]. Another important property of QCD is the asymptotic freedom [17], for which the bond between particles becomes weaker for larger energies or smaller distances. Figure 1 shows the strong coupling constant α_s as a function of the kinematic energy scale Q that can be understood as the inverse distance scale in hard process [18]:

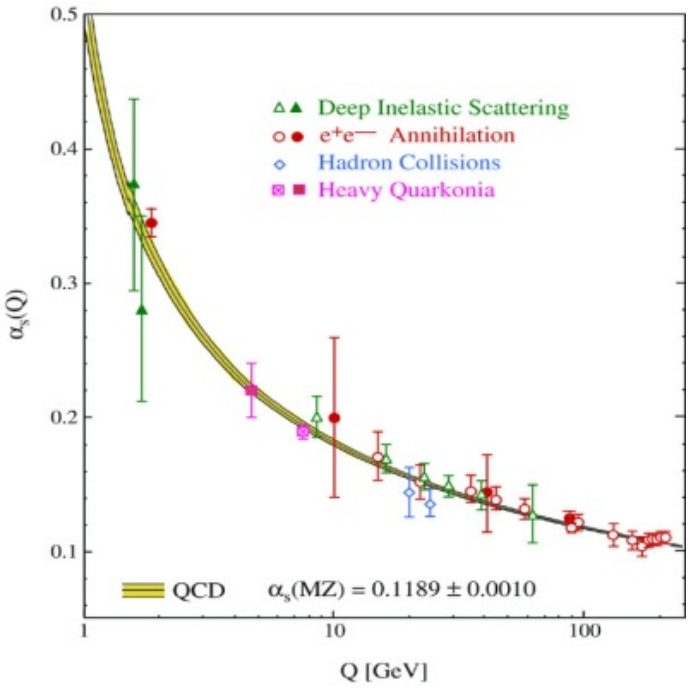

Figure 1: Figure that shows the dependence of the strong coupling constant α_s with respect to the kinematic energy scale Q. This coupling α_s in QCD is the equivalent to the electric charge in the electromagnetism. The scale Q is just a measure of the energy of the process. For low energy, the coupling becomes large; and for high energy it becomes small.

An interaction with high energy means that is an interaction that happens in short distance, and a phenomena with small energy means that is happens in long distance. Thus,

[1] Photons do not interact in the leading order of the perturbative expansion. In next-to-leading order, two photons can interact via fermion loop described by so called box diagram [15].

it is possible to classify the phenomena in short and long range phenomena depending on the typical interaction scale. It is possible to describe the large scale phenomena ($Q \gg 1$ GeV) by applying perturbation theory [19], but for low scale $Q \sim \Lambda_{\text{QCD}} \approx 200$ MeV phenomena one has to rely on experimental data.

QCD is a part of the called Standard Model of particles [20], together with Quantum electrodynamics, and is one of the theories that has endured many tests in the whole field of physics.

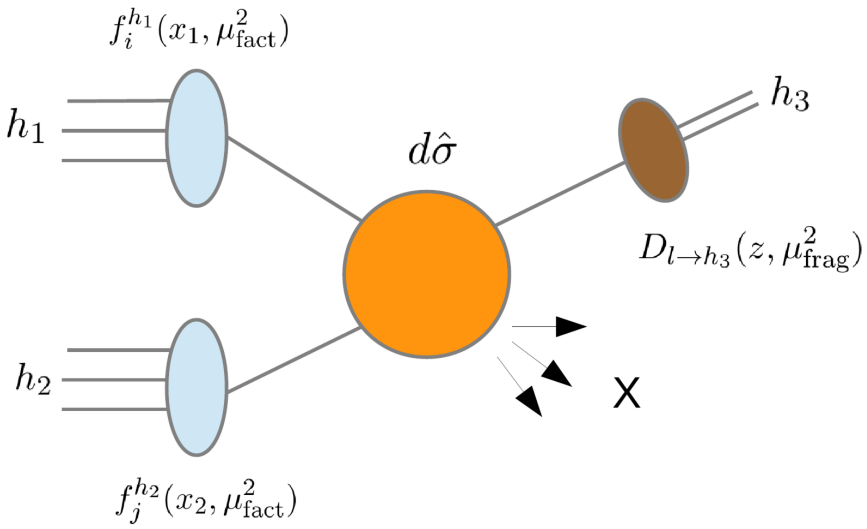

Figure 2: Collinear factorization schematic. It presents inclusive production of the hadron h_3 when two hadrons, h_1 and h_2, interact. The $f_{i,j}^{h_1,h_2}(x_1, Q_p^2)$ are the parton distribution functions, stating the probability of finding a parton i or j in the hadrons h_1 or h_2; the $d\hat{\sigma}$ is the partonic cross section, describes how the partons i and j interact with each other; and finally $D_{l\to h_3}(z, \mu^2_{frag})$, explains how a parton l, product of the interaction, fragments into another hadron h_3. This figure is taken from [21].

In order to study most of the QCD properties, the main process used are the proton-proton

collisions. In Figure 2 is shown a simple schema on this process [22]. In the left hand side are the incoming protons (which are hadrons with three quarks [23]), called h_1 and h_2. Each of this protons contribute with one parton (which can be a quark or a gluon) i and j. The probability of finding a parton i in the hadron h_1 is given by the parton distribution function (PDF) [24] $f_i(x_1, Q_p^2)$ and respectively the probability of finding a parton j in the hadron h_2 is given by the parton distribution function $f_j(x_2, Q_p^2)$. The PDFs describe the structure of free proton in rest, that is a long range phenomena. PDFs cannot be obtained from QCD with perturbation theory, and hence that they are non-perturbative. They can be determined experimentally mainly from the deep inelastic scattering data [24], since it is a high energy phenomena, the coupling constant becomes small and the QCD processes become important.

The next part is the interaction between these partons, described by $d\sigma^{ij\to k+X}$, which is called the partonic cross section [25]. You can view the partonic cross section as a (dimensional) probability that a parton k is produced in the scattering of partons i and j. The cross section is inclusive, meaning we do not measure what else (anything, X) is produced at the same time. It is known that the scattered parton k will start to fragment after the collision and those fragments will combine to produce hadrons. All the hadrons coming from the scattered parton form a collimated cone of particles named a jet. This phenomena is explained by the fragmentation function [26] $D_{k\to h_3}(z, Q_F^2)$, and would read as the probability, for scattered parton k, to form a hadron of type h_3. All the described quantities are assembled together in the collinear factorization theorem [27]:

$$d\sigma^{h_1h_2\to h_3+X} = \underbrace{\sum_{ijk} f_i(x_1, Q_p^2) \otimes f_j(x_2, Q_p^2) \otimes d\sigma^{ij\to k+X}}_{\text{Jet cross section}} \otimes \underbrace{D_{k\to h_3}(z, Q_F^2)}_{\text{Fragmentation function}} \tag{1}$$

where x stands for the momentum fraction of the interacting partons 1 and 2, $Q_{F/p}^2$ are scale factors, and z is momentum fraction 3 with respect to the jet momentum. When doing QCD calculations it is assumed that $Q_F^2 = Q_p^2 = Q_{hard}$ for simplicity. The convolution of

the parton distribution functions and the partonic cross section is the jet cross section. After the scattering process, the result is a bunch of particles, forming a collimated cone. This is called jet in high energy particle physics, as stated before. In Figure 3 is shown an example on how a jet could look experimental. There the green tracks would correspond to particles that belong to the jet and the grey cone shaped volume correspond to the geometrical definition of the cone (how this is done can be found in Chapter 5). The momentum of the jet is calculated summing the momenta from all the particles in the jet. The momentum of the jet defines the jet axis, to which we can relate the momentum of each and every particle in it. The contribution perpendicular to the axis is called j_T, but the study of j_T goes beyond the scope of this thesis, but it has been widely studied [28,29]. In the Equation 1 is shown that $D_{k\to h_3}(z, Q_F^2)$ only depends on Q_F^2, which is a scale factor, and z, which is a kinematic variable, describing the longitudinal momentum fraction with respect to the jet axis. The mathematical definition is, as ATLAS experiment uses [30]:

$$z = \frac{p_{jet} \cdot p_{ch}}{|p_{jet}|^2} \tag{2}$$

where $p_{\mathrm{T,jet}}$is the total momentum of the jet and p_{ch} is the momentum of the charged particle we are studying. An important feature of the fragmentation function is that it does not depend on the incoming hadrons of the hard process, but it depends only on what is the flavor k of the fragmenting parton. Hence it is said that fragmentation function is an universal function.

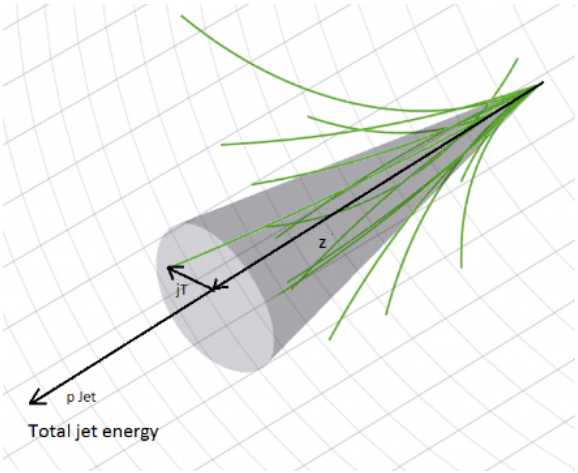

Figure 3: Vector $\vec{P}$ stands for the total momentum of the jet and gives the direction of the jet axis. Momentum fraction of a constituent in the jet along the jet axis is given by z. This variable z is the same as in the fragmentation function dependence, $D_{k\to h_3}(z, Q_F^2)$, and will be the nucleus of this analysis. Similarly the jet transverse momentum j_T is the projection of constituents momentum perpendicular to the jet axis.

For this study, I have tested a model presented by Feynman and Field [31] with new proton-proton data on the fragmentation function, produced by the ATLAS collaboration [32] in 2011. This study included the comparison of several Monte Carlo samples with the data, but the data was limited with large error bars. This motivated the use of the PYTHIA event generator, one of the available event generators, to test the data, and use it to improve the quality of a fit in further analysis.

In this work I will produce simulated data with the help of a Monte Carlo simulator, PYTHIA8 8.212, I will compare it to the real data from ATLAS, and then I will test the Feynman and Field model with the data produced by the simulation.

The following chapters are organized in the following way. In Chapter 2 I introduce the cascade model proposed by Feynman and Field, to simulate the fragmentation function. Then I will introduce ATLAS experiment in Chapter 3, where I describe the details of the

experimental setups for the jet analysis. I will explain the jet reconstruction method used in Chapter 4. Next in Chapter 5 the PYTHIA event generator is presented, with all the details on the parameter settings of pythia and jet reconstruction parameters used for the analysis. At the end the results are shown and the conclusions made. I will finish with my results and conclusions in Chapters 6 and 7.

2 Fragmentation Function

2.1 Fragmentation function

As discussed in the introduction, the fragmentation function $D_{k\to h_3}(z, Q_F^2)$ is the function that describes the hadronization of the products of a deep inelastic scattering process. After the scattered parton starts to move away from the collision center, the coupling constant (α_s) starts to become larger and larger until there is enough potential energy to start producing pairs of quark anti-quark to satisfy the color confinement. Some useful relations that the fragmentation function must fulfill are [33]:

$$\sum_{h_3} \int_0^1 z D_{k\to h_3}(z) dz = 1 \tag{3}$$

$$\sum_{k} \int_{z_{min}}^1 D_{k\to h_3}(z) dz = n_{h_3} \tag{4}$$

where z_{min} is the minimum energy for producing the hadron h_3. The first equation basically means that the sum of the energy of all the products of the fragmentation must be equal to the energy of the initial fragmented scattered parton. The second equation shows how many hadrons of type h_3 are produced for all scattered partons k.

2.2 Feynman and Field model

In 1970s, Feynman and Field [31] presented a model that tries to explain how a parton originating from a proton-proton collision will fragment into other partons. The model includes a full flavor description, but the focus in this work will be the kinematic part. The idea is to reproduce the fragmentation through a sequential cascade of particles. Figure 4 illustrates how the cascade is build in this model.

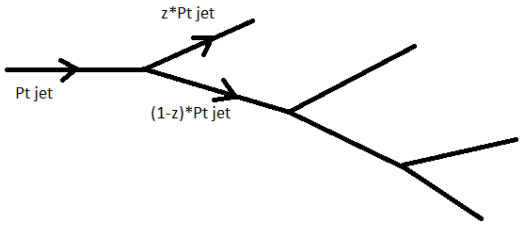

Figure 4: Cascading model by Feynman and Field.

The idea is that the parton initiating the cascade starts to split into lower energy partons. This splitting is described by the probability distribution $f(z)$ that assigns the momentum fraction z to each splitting such that $z * p_{T,jet}$ is the momentum of the first outgoing hadron from the jet and $(1-z) * p_{T,jet}$ is momenta left for the next splitting. The splitting of the cascade continues as long as the remaining momentum is higher than a predefined cut of scale.

In order to be implemented, this model requires the knowledge of the splitting probability $f(z)$ to be made. This is different from the fragmentation function (FF), since the integral of the FF is not 1, but it is $\int_0^1 D_{k\to h_3}(z, Q_F^2)dz$ = number of hadrons of type h_3 in the jet, as explained in the previous subsection. Nevertheless Feynman and Field were able to relate these two quantities using an integral equation:

$$F(z)dz = f(1-z)dz + \int_0^{1-z} dz_1 f(1-z_1)F(\frac{z}{1-z_1})d(\frac{z}{1-z_1}), \tag{5}$$

where the F(z) is

$$F(z) = \frac{1}{N_{jets}}\frac{dN_{ch}}{dz} \tag{6}$$

The first term represents the probability that the first particle on the decay leaves the momentum fraction $\eta = 1 - z$ to the remaining cascade. In the second term z_1 represents the momentum fraction that the first particle takes as integration variable. If the first particle takes a momentum $z_1 > 1 - z$ the value of the integral will be zero, since it is not possible that any other particle gets the chance of achieving enough momentum

fraction. For instance, if we want to know the probability of a particle getting $z = 0.7$, that would be the probability for the first particle $f(0.3)$ plus for the rest of the particles if the first particle takes a momentum fraction between 0 and 0.3. The integrand accounts for the probability that some particle gets a momentum fraction z if the first particle takes momentum z_1 $(F(\frac{z}{1-z_1})d(\frac{z}{1-z_1}))$, weighted with the probability of the first particle taking that momentum z_1 $(f(1-z_1))$.

3 ATLAS experiment

3.1 ATLAS detector

ATLAS (A Toroidal LHC Apparatus) [34] is one of the major experiments, together with ALICE (A Large Ion Collider Experiment) [35], CMS (Compact Muon Solenoid) [36] and LHCb (LHC-beauty) [37], located at the LHC (Large Hadron Collider) in Geneva. The main goals of ATLAS experiments are to search for new particles and for new interactions beyond the standard model, together with CMS. It is made of a set of detectors with different purposes.

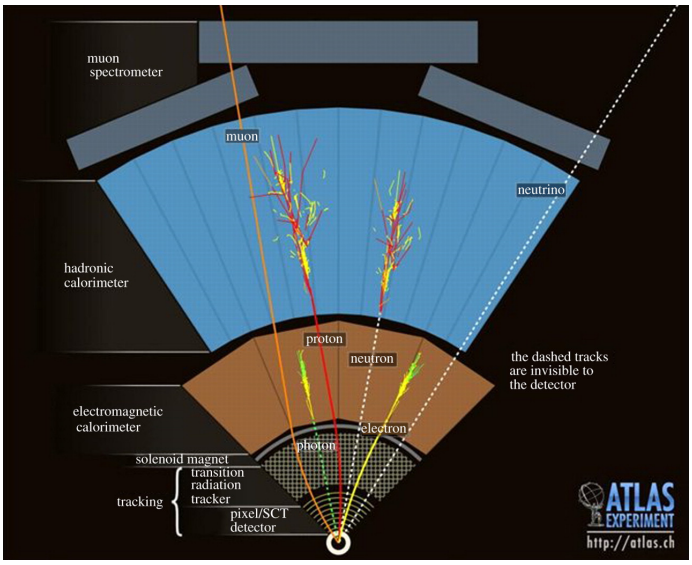

Figure 5: Schema of the different detector parts of the ATLAS experiment, where the blue part corresponds to the hadronic calorimeter (measurement of the energy of the hadrons), the brown part is the electromagnetic calorimeter (measurement of the energy of all the electric charged particles, and the inner detectors track the momenta of the electric charged particles.[2]

The ATLAS detector is of special importance for this thesis since the data used is from it. Figure 5 shows a schema on the different detectors that compound ATLAS experiment and it illustrates how the different particles interact with the different type of detectors. The inner detectors, the yellow lines and the grid, are trackers for charged particles to measure the momenta of charged particles. This is done through a magnetic field, that bends the trajectories of the charged particles, and thus is possible to know the momenta. The trajectory of the particles are usually measured using gas detectors, that the detect the ionization produced by the passing of a charged particle[3] [14].
The next detector is the electromagnetic calorimeter [14], the brown region on the figure. This device is used to detect electrons and photons, and gives a good measure of the energy of those particles. Keeping the same order, from inner detectors to outer detectors, the next detector is the hadronic calorimeter in the blue region. It has the same function as the electromagnetic calorimeter, but for the hadrons, such as neutrons or protons[4]. Usually calorimeters have two components, absorber material and active material. When a particle enters the calorimeter reacts with the absorber material and leaves energy in the active material. Later the energy is summed and thus obtaining the energy of the original incoming particle. ATLAS calorimeters are composed by: steel as the absorber material, and scintillating tiles as active material. The full description about each detector can be found at [34].

ATLAS has done a study [32] in which, for reconstruction of the jets, all particles detected are used. All kinematic calculations are done using charged tracks since tracker detectors provide the best momentum information for the observed particles. The results obtained are compared to different event generators such as PYTHIA [38] and Herwig [39]. In a part of this thesis I will do the same analysis, trying to reproduce as closely as possible

[2] $http://stanford.edu/group/stanford\_atlas/4Particle\%20Collision\%20and\%20Detection$
[3] http://atlas.cern/discover/detector/inner-detector
[4] http://atlas.cern/discover/detector/calorimeter

this ATLAS experiment.

A typical di-jet event, measured in a proton-proton collisions, is presented in Figure 6. The part at the left-top corner shows the event from the beam axis perspective, and shows the transverse plane. The momentum the particle has in this plane is called as the transverse momentum, p_T. The left-low corner shows another section of the same event, in this case the protons come from the left and right and collide in the center. In these two pictures it is possible to distinguish the different detectors in the experiment. The central dark region, where the lines with color appear is the tracker detector. Next, the green region corresponds to the electromagnetic calorimeter. The remaining red region is the hadronic calorimeters. All the yellow tiles on the calorimeters show where particles are detected. The right corner corresponds to the measurement in a calorimeter, all circles in the plane are jets that the anti-k_T algorithm gives out. This is a typical di-jet event; with two leading jets, the two yellow towers, and the rest with small energies.

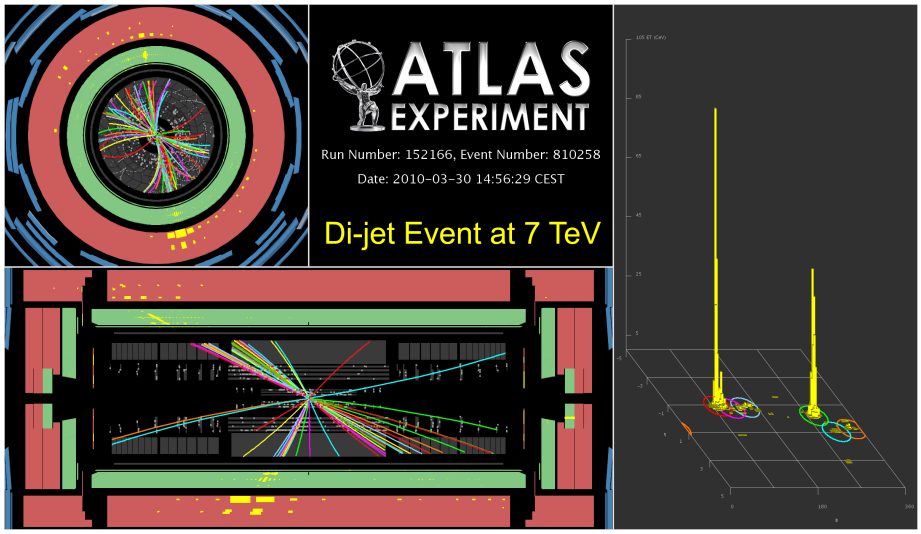

Figure 6: This example shows a di-jet event measured by ATLAS collaboration in a proton-proton collision at $\sqrt{s} = 7$ TeV. In the left hand side, the upper figure shows the transverse view, and the lower figure the longitudinal view, of the collision. Colored lines are tracks of charged particles, and yellow boxes hits to the calorimeter towers. Figure at right shows the energy deposited into calorimeter towers in (ϕ, η) plane and circles present the area of jets reconstructed by the jet algorithm. Figure is taken from www-page [5].

[5] *https : //twiki.cern.ch/twiki/pub/AtlasPublic/EventDisplayFirstCollisions7TeV/ATLAS*2010_152166_810258.*png*

4 Jet Reconstruction

4.1 Jet Definition

One of the key concept in high energy physics is the idea of jets. The notion of jet correspond to a shower of particles in a very narrow cone, product of a collision of particles at very high energy [40].

The first thing that should be done is to define what a jet is. After the process described for the jet cross section in the collinear factorization, the scattered parton starts to fragment into other partons. This is known as the partonic shower [41]. In Figure 7 this would be the area right next to the collision, where the splitting into quarks and gluons happens. The next step is the hadronization of this partons [42]. All the particles that carry color charge are affected by the color confinement, and this phenomenon forces quarks and gluons to unite in order to be colorless hadrons [43]. According to Feynman [31], also pairs of quark-antiquarks are created in this process to fulfill this condition. This way, all the hadrons whose mother is the original scattered parton will form a jet.

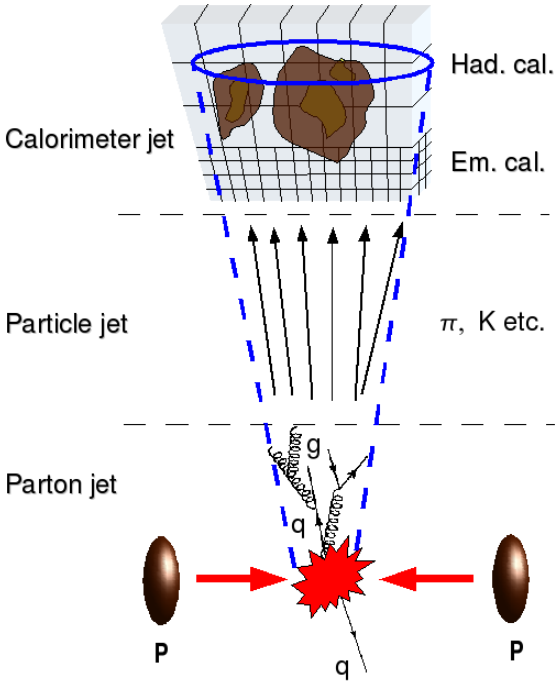

Figure 7: Representation of a proton-proton collision and the different stages in the formation of jets. After the collision the scattered parton starts to fragment into more partons that later hadronize and form the jet. Figure taken from [44].

In an experiment jets are defined in different ways. In the proton-proton collision, there are many particles that do not originate from fragmentation of the hard parton. These uncorrelated particles are the result of the underlying event. This underlying event consists mostly from the beam remnants, the parts of the protons that do not interact. Other forms of underlying event are multiple interactions or soft processes [45]. During a proton-proton collision, the parton interacting also radiate, and this phenomena is known as initial and final state radiation, depending if it happens before or after the hard process respectively. Figure 8 shows this schematically.

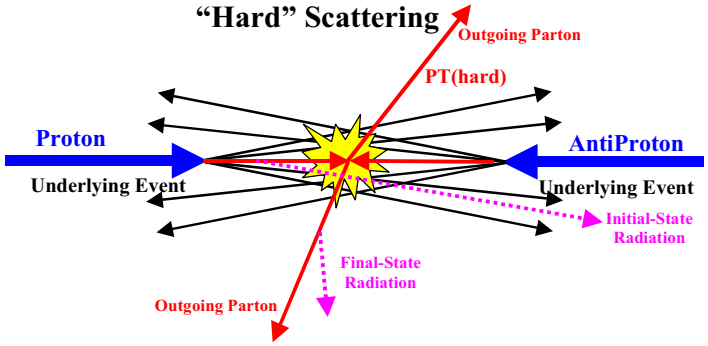

Figure 8: Schematic view of the proton-(anti)proton event. The blue arrows are incoming beams, red and magenta arrows depict the hard physics in the event and black arrows represent the underlying event. Figure is taken from [45].

4.2 Reconstruction algorithms

To solve the classification of particles into jets, the solution is the application of a certain algorithm to reconstruct the jets. Depending on how these algorithms classify the particles into jets, they are divided into two main groups [46]: cone algorithms and sequential recombination algorithms.

The cone algorithms are based on the idea of a rigid cone in the $\eta - \phi$ plane, being η the pseudorapidity and ϕ the azimuthal angle. The most simple cone algorithm searches for the most energetic hadron in the final list of particles, and defines a cone around it, using the parameter R. This R is the cone radius in the $\eta - \phi$ plane, and therefore defines an area $A = \pi R^2$. All the hadron trajectories inside that area would belong to the jet.

The sequential recombination algorithms more based on the idea of recombining particles. In this particular study, the important algorithms are the k_T algorithms [47]. The k_T algorithms are defined using the distance between particles d_{ij} and the distance from every particle to the beam axis d_{iB} using the following formulas:

$$d_{ij} = min(k_{ti}^{2p}, k_{tj}^{2p}) \frac{\Delta_{ij}^2}{R^2}, \tag{7}$$

$$d_{iB} = k_{ti}^{2p}, \tag{8}$$

where $\Delta_{ij}^2 = (y_i - y_j)^2 + (\phi_i - \phi_j)^2$, k_{ti} is the transverse momentum, y_i is the rapidity and ϕ_i is the azimuth of the particle i. R is also a parameter given and p defines what type of algorithm is used. The algorithm starts by defining both quantities for every particle, which now become protojets. From all the calculated distances, the algorithm picks the smallest one. If it is a distance between two particles d_{ij} the algorithm merges both particles defining a new protojet. If the smallest distance is a d_{iB} the protojet is "not mergable", becomes a final jet, and is taken out from the protojet list. This algorithm is repeated until there are no more protojets.

With $p = 1$ it corresponds the k_T algorithm, with $p = 0$ it corresponds the Cambridge/Aachen [48] algorithm and with $p = -1$ it corresponds the anti$-k_T$ algorithm [49]. For our simulation the algorithm used was the anti$-k_T$ algorithm, as ATLAS did on their analysis.

5 PYTHIA Event Generator

5.1 ATLAS characteristics

In order to reproduce the data from ATLAS I need to know the limitations of the detector, and implement them in the simulation. In the ATLAS measurement paper [32] the following acceptance of the particles and the parameters of the jet reconstruction algorithm were taken into account in the measurement and the following simulations:

- Jet p_{T} cut: $p_{\mathrm{T,jet}} > 20$ GeV, this cut is applied in order to discard jets that are not product of the hard process.
- Particle energy cut: minimum p_{T} cut is required,$p_{\mathrm{T}}track > 0.5$ GeV,
- η Acceptance: $|\eta_{\mathrm{particles}}| < 1.8$, where $\eta_{\mathrm{particles}}$ is the pseudorapidity of the particles, and it is required to be less than 1.8 to enter into the jet reconstruction. Taking this into account, if jets with radius $R = 0.6$ are considered, then $|eta_{jet}| < |eta_{particles}| - R \Rightarrow |\eta_{jet}| < 1.2$, this is called the fiducial acceptance.
- Charged Particles: Only charged particles will be used for the kinematic analysis.

5.2 PYTHIA event generator

PYTHIA [38] is a particle physics collision event generator, able to generate proton-proton collision events given certain parameters such as incoming particles, energy of the particles, number of events to simulate or decay criteria. Some other settings can be also applied to enhance certain characteristics the researcher might be interested in. This tool is widely used nowadays in the particle physics field. For this study the version used was PYTHIA8.2.1.2.

5.2.1 Configuration file

In order to run the simulation, PYTHIA can use a configuration file, detailing information regarding the process studied. The use of configuration files make PYTHIA more flexible, allowing to make the same simulation with different parameters, and not having to recompile the code in just to change some configuration. For the purposes of this thesis the following main parameters where set in order to reproduce the ATLAS data:

- Random Number Seed (Random:setSeed): This feature should be turned on and given a value on Random:seed to generate a random number sequence for the Monte Carlo simulation.

- Beam ID (Beams:id(A or B)): Beam ID stands for what kind of particle is colliding in the simulation. In the case of a proton to proton collision would be Beams:idA = 2212 and Beams:idB = 2212

- HardQCD : HardQCD setting is on, so all QCD jets and jet processes are possible, and the diffractive events are not simulated.

- pTHard (PhaseSpace:mHat): With this setting you can enrich the hard jet events in the produced sample. This setting forces all outcoming partons from the hard process to have $p_{\mathrm{T}} > 15$ GeV/c. This setting is discussed in detail later.

- Particle decay: Finally, this states if a particle can be consider stable or if it decays. All particles with a lifetime shorter than tau0Max (mm/c) will decay. In order to reproduce ATLAS results, it was used: ParticleDecays:limitTau0 = On and ParticleDecays:tau0Max = 10.0.

5.2.2 Code structure

After including the appropriate headers in the code to make PYTHIA work, the data from the configuration file is read. The next step is to create a loop to initiate the events. Once

the event is created, some cuts are applied. Firstly, some histograms are filled with all the final state particles in the event, or in other words the particles do not decay before they are detected. Also a minimum p_{T} cut is made for all particles, in this case $p_{T,min} = 0.5$ GeV; and pseudorapidity cut is also made, $|\eta| = 1.8$. All these cuts are made in accordance with the ones described in ATLAS measurements [32].

Following to the cuts, it is possible to extract and store the information regarding the outgoing particles in vectors called PseudoJet. If a particle fulfills the above requirements, then the main attributes are written in a vector. This vector includes the energy and the three momentum of each particle. Then the vector is added to a list of final state particles, which will be used to reconstruct the jets.

5.3 Particle selection

When simulating collisions, PYTHIA generates an event and a list of all particles according with the configuration file. In the configuration file it is written specifically the 'ParticleDecays' configuration. According to the PYTHIA documentation[6] this class is in charge of the decays of all unstable hadrons. By activating this feature a limit is set to the particles that can be detected. Specifically the parameter was set to be $\tau_{0Max} = 10.0$ mm/c. Thus all the particles with a lifetime shorter than 10.0 mm/c$\approx \frac{1}{3}10^{-10}$s will decay. This means that π^0, with lifetime 8.4×10^{-17}s will decay. This represents a challenge experimentally since it is difficult to say whether a photon comes from a decay or from something else. This is another reason to justify the use only of charged particles in the kinematic analysis.

The next part of the code is the jet reconstruction. The anti$-k_T$ algorithm is the method used in ATLAS experiment, and also for this study. The algorithm was implemented in the FastJet package [50] and called inside the PYTHIA code. I used the same R parameter value as ATLAS did $R = 0.6$.

[6] $http://home.thep.lu.se/\ torbjorn/pythia81html/ParticleDecays.html$

5.4 Time estimation and $p_{\mathrm{T,hard}}$

The p_{T} spectra is used as one of the sanity checks of the simulation. It has a typical exponential shape in low p_{T} and powerlaw shape in high p_{T}, which is the interesting region for this study. In order to compare the results of the simulation on fragmentation function, is important to first analyze how well the simulation reproduces the experimental p_{T} spectra.

During the construction of the code it was necessary to estimate how much time would take a simulation to produce significant statistics. Taking advantage of the powerlaw form of the p_{T} spectra, it is possible to predict how long it will take to produce a certain amount of statistics in a p_{T} region. This can be done by fitting the spectra with an powerlaw shape, and knowing the time that took to get certain amount of data, extrapolate and calculate how much time would be needed to get the amount of data wanted. The conclusion of that analysis was that using minimum-bias simulation ($p_{\mathrm{T,hard}} = 0$ GeV) would take a considerably long period of time, so in order to have enough data it is required to add a new parameter to the simulation.

The $p_{\mathrm{T,hard}}$ is a convenient feature of PYTHIA for this purpose. As described before it enhances the production of higher p_{T} phenomena by raising the invariant p_{T}. This reduces considerably the time needed by the simulation to reach certain p_{T} regions, which makes it useful for this kind of study. The usage of this feature shifts the spectra towards higher p_{T}, and this changes the p_{T} spectra as shown in the left part of Figure 9. The minimum-bias p_{T} spectra presents closely an powerlaw trend for all p_{T}. Nevertheless, for a non-zero $p_{\mathrm{T,hard}}$ ($p_{\mathrm{T,hard}} = 15$ GeV in the figure), at low p_{T} regions the spectra has a peak, around $p_{\mathrm{T}} = 15$ GeV, and then starts to decrease until resembles an powerlaw trend. It is necessary to make sure that the usage of this feature does not affect the shape of the pt region used for the analysis.

In order to use a simulation with $p_{\mathrm{T,hard}} = 15$ GeV it is sufficient to compare the p_{T} spectra with a minimum biased simulation and determine the difference as a scaling factor. The left

hand side of the Figure 9 shows the both spectras together, enhancing the $p_{\mathrm{T,hard}} = 0$ GeV one by a factor of 800, and is possible to conclude that the high p_{T}power is not modified by this $p_{\mathrm{T,hard}}$requirement. Thus is possible to assume that no distortions will appear in the jet spectra in the range of study, and the data generated with $p_{\mathrm{T,hard}} > 15$ GeV.

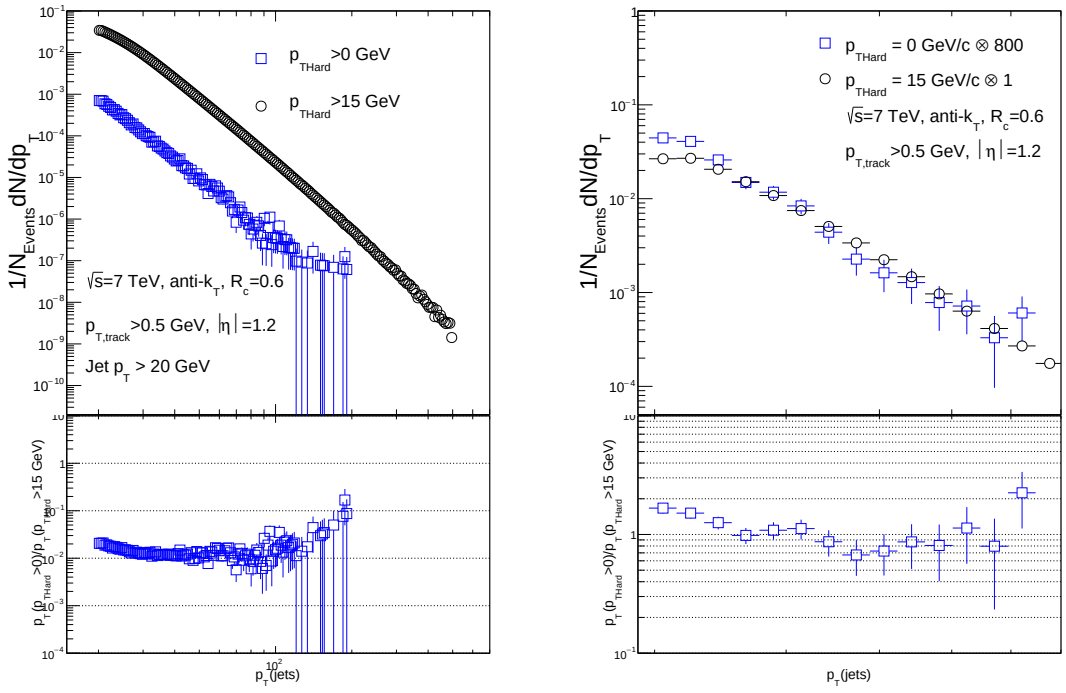

Figure 9: The left panel shows the p_{T} distribution for $p_{\mathrm{T,hard}} = 0$ (blue squares) and $p_{\mathrm{T,hard}} = 15$ GeV/c (black circles). It is clear that higher $p_{\mathrm{T,hard}}$ enriches the high-p_{T}jet production. The right panel shows the same except that $p_{\mathrm{T,hard}} = 0$ spectrum is scaled by a factor of 800 and histograms are rebinned in order to reduce the statistical fluctuations between $19 < p_{\mathrm{T,jet}} < 70$ GeV.

6 Results

6.1 PYTHIA simulation validation

Once the $p_{\mathrm{T,hard}}$ setting is proven safe, is necessary to make sure the simulation is producing the results we are interested in. To justify the simulation two observables can be analyzed: the rapidity and the p_{T}. This is not only to confirm the result but also in case of finding disagreements, these tests can indicate what causes them.

6.1.1 Rapidity distributions

The rapidity variable is related to the relativistic velocity. In particle physics the rapidity is commonly defined using:

$$y = \frac{1}{2} \ln \frac{E + p_z}{E - p_z} \tag{9}$$

where E is energy and p_z is the longitudinal momentum of the particle along the beam axis. Rapidity is related with longitudinal velocity, as $y \to v_z/c$, when $v_z/c \ll 1$, but it is convenient in relativistic calculations since it is additive in longitudinal Lorentz transformations. At the ultrarelativistic limit rapidity coincides with pseudo-rapidity, i.e. $y \to \eta$, when $m/E \ll 1$. As the pseudorapidity is directly related with scattering angle, it is easier to access it experimentally. The rapidity distribution for the simulation is presented in Figure 10.

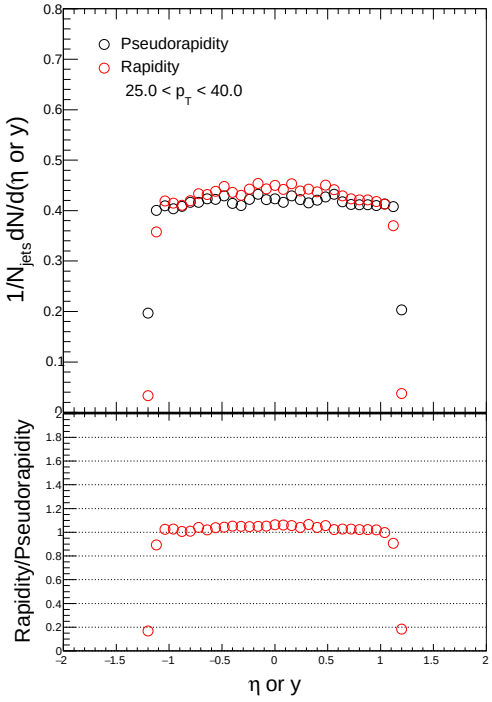

Figure 10: Rapidity (red) and pseudorapidity (black) distributions of jets in the lowest jet transverse momentum bin, $25 < p_{\mathrm{T,jet}} < 40$ GeV and their ratio. One observes that there is no significant difference between them in these jet energies. For higher jet energies the distributions become noisy due to the lack of jets in those energies.

6.1.2 p_T distributions

The other test of the simulation is comparing the p_T distribution of the simulation to the results obtained by ATLAS. In the simulation this is done by creating a histogram with the transverse momentum p_T values of the jets and comparing it to the ATLAS measurement. In order to do the comparison it is required to make sure that both distributions are in the same units. ATLAS $p_{\mathrm{T,jet}}$ spectra are in $\frac{d\sigma}{dp_T dy}$ [pb/GeV] and PYTHIA are in $\frac{1}{N_{\mathrm{events}}}\frac{dN}{dp_T}$. This two quantities can be related using the following equation [51]:

$$\frac{d\sigma}{dp_{\mathrm{T,jet}}dy}\,[\mathrm{pb/GeV}] = \frac{\sigma_{\mathrm{gen}}}{N_{\mathrm{accepted}}}\frac{1}{\Delta\eta}\frac{dN}{dp_{\mathrm{T,jet}}} \tag{10}$$

where σ_{gen} is related to the cross section given in milibarns (here is included the contribution of the $p_{\mathrm{T,hard}}$), N_{accepted} stands for the amount of events accepted to be simulated [38]. This are values the PYTHIA simulation provides. There is also $\Delta\eta$ stands for the pseudorapidity value ($\Delta\eta = \eta_{max} - \eta_{min}$). Figure 11 shows the comparison of measured and simulated p_{T} distribution of jets. Neither in my simulation or in ATLAS data the underlying event was subtracted. The original data from ATLAS [30] had $|y = 0.3|$ thus, a run of the simulation was made only generating the jet p_T spectra to compare with the ATLAS jet p_T spectra.

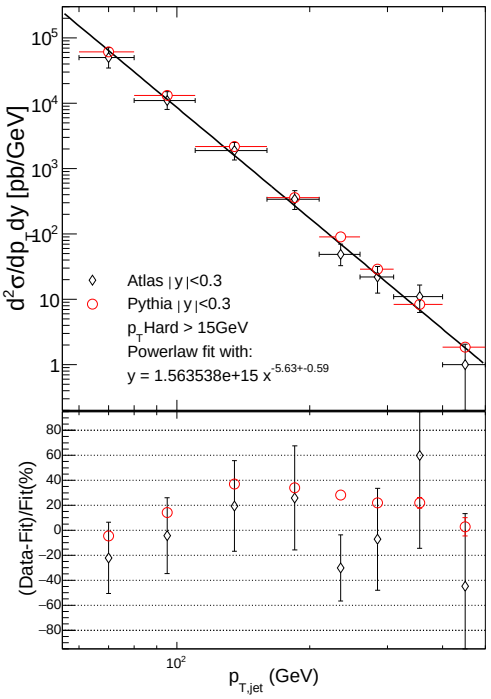

Figure 11: Jet cross section in $|y| < 0.3$ measure by ATLAS [30] as compared to PYTHIA simulation made using $p_{\mathrm{T,hard}} > 15$ GeV. The solid line is a powerlaw fit to the ATLAS data and lower panel shows the ratio of the data and the PYTHIA simulation to the fit. The values that scales the simulation p_{T} distribution is obtained through the Equation 10.

6.2 Z-distributions comparison

Once the p_{T} and the rapidity distributions are done, the next step is to compare the z-distributions. As defined before, the z-distribution show the part of the momentum a certain particle takes from the jet during the fragmentation process. Figure 12 left hand side shows the fragmentation function in bin $25 < p_{\mathrm{T,jet}} < 40$ GeV measured by ATLAS (black circles) [32] and my PYTHIA simulation (red circles). Lower panel shows how much PYTHIA results deviate from the measured data. PYTHIA and the data

agree within 20% for all z ranges, for all $p_{\mathrm{T,jet}}$ energies. Right hand side in Figure 12 is taken from [32] and it shows the comparison to many different event generators and their tunes, made by ATLAS. The PYTHIA8.2.1.2 results from this work on the left panel agree well to the PYTHIA8.1.4.5 used for ATLAS paper shown on the right panel; with both event generators overestimating the fragmentation function in low z region, and also underestimating for high z region. The results from other jet momentum bins can be found in Appendix A. For increasing $p_{\mathrm{T,jet}}$ energies, the overestimation in low z region of the fragmentation function maximum appears in lowers z's, and the underestimation tends to get slightly bigger.

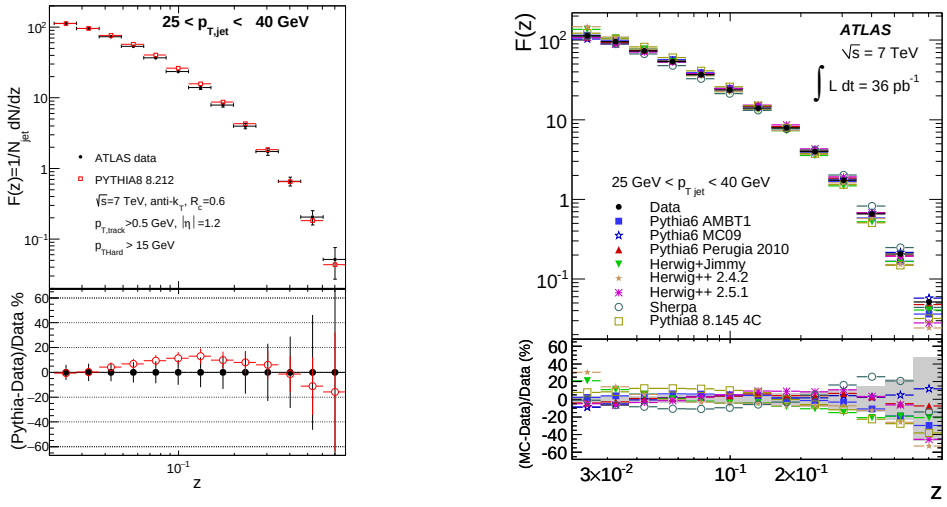

Figure 12: Left Figure shows the ATLAS results for fragmentation function (solid black) for jets $25 < p_{\mathrm{T,jet}} < 40$ GeV [32]. Red open circles are results from my PYTHIA simulation. Lower panel shows how much the simulation deviates from experimental results (%). The right Figure is made by ATLAS [32] and presents the same for different event generators and their tunes. The same results in different jet momentum bins are presented in Appendix A.

Figure 13 shows a comparison of the z-distributions for all the different $p_{\mathrm{T,jet}}$ energies for my PYTHIA simulation on the left panel, and the ATLAS on the right panel. As has been said, the fragmentation function, $D_{k\to h_3}(z, Q_F^2)$, depends on the z variable, but also on the Q_F^2 scaling. The $p_{\mathrm{T,jet}}$ dependance observed in Figure 13 is a manifestation of this dependance with respect the Q_F^2 scaling. The simplest parton model would predict a scale independent $D = D(z)$, but perturbative quantum chromodynamics corrects this and shows logarithmic scaling violations [52]. As shown at the ratio panel on both figures, the lower $p_{\mathrm{T,jet}}$ energies tend to have lower values for smaller z, and also to peak around $z = 0.3$. For higher $p_{\mathrm{T,jet}}$ energies the differences start to be small. Nevertheless one observes that the differences between the simulation and the experimental data are within 20%.

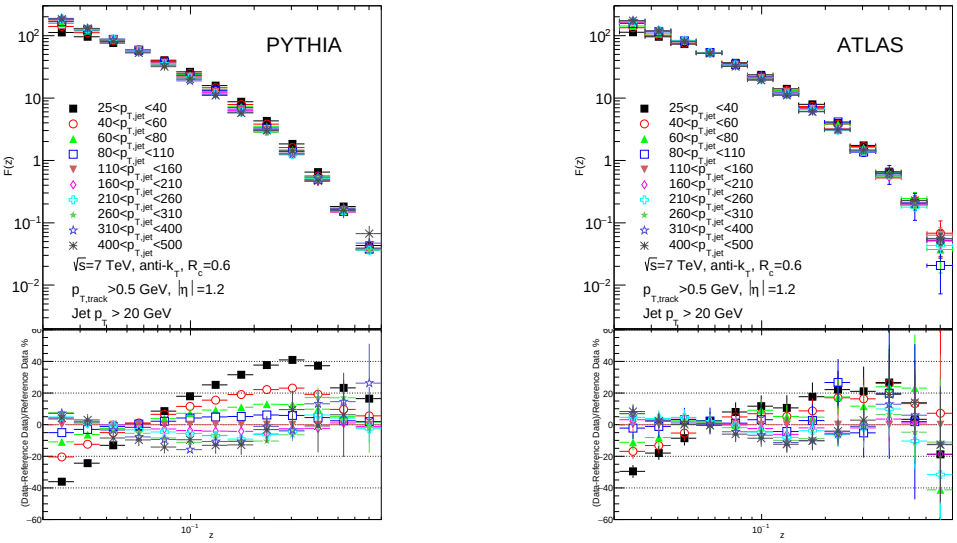

Figure 13: Fragmentation function in different jet transverse momentum ($p_{\mathrm{T,jet}}$) bins. Left Figure shows the results from my PYTHIA simulation. Lower panel shows the ratio to the bin $110 < p_{\mathrm{T,jet}} < 160$ GeV. Right Figure shows the same but for ATLAS data [32].

FF parameter limits	Norm	α	β	γ
Top limit	20	50	10	50
Low limit	0	0	0.1	0.1

Table 1: Table showing the limits applied to the parameters of the KKP parametrization. On the top row are the name of the parameters, the next row shows the higher limit this parameters can take, and the last row shows the lower limit for the parameters.

6.3 Splitting probability analysis

The final part of the analysis is the test of the Feynman and Field cascading model. For this purpose the following procedure was followed. First the PYTHIA simulation data was fitted using the called KKP parametrization [53] form:

$$F(z) = Nz^{-\alpha}(1+z)^{\beta}(1-z)^{\gamma} \tag{11}$$

This form includes three parameters (α,β and γ); where the $z^{-\alpha}$ term is dominating at low z; $(1-z)^{\gamma}$ dominates at high z, shrinking the function towards $F(z) = 0$; and finally $(1+z)^{\beta}$ term modules in intermediate z ranges. It was not possible to fit over the whole range of z, because the fit became unstable if the fitting range was extended below z = 0.03. Hence the final fitting range was $0.03 < z < 0.99$. In the plots, the fit is represented using a solid black line. When doing the fits, some limits were applied to the parameters in order to avoid strange solutions. The limits to the KKP parametrization fit are shown in Table 1. Those limits are purely empirical, in order to get results:

Tables 2 and 3 shows examples of the values obtained from the fit. Three different fragmentation function data were used: ATLAS [32], PYTHIA simulation using same z binning as ATLAS, and using finer bins especially in higher z ranges for $0 < z < 1$.

Most of the parameters show agreement for the different initial data. This makes the process more reliable.

$p_{\mathrm{T,jet}} = 25 < p_T < 40GeV$	Norm	α	β	γ
ATLAS data	15.2816	0.643743	0.0100002	11.037
PYTHIA Atlas bin	20	0.576186	0.726743	10.5294
PYTHIA Log bin	20	0.578006	0.765603	10.6373

Table 2: Table showing example of the values after the fit procedure for each different fragmentation function data, according to equation 11 for $25 < p_{\mathrm{T,jet}} < 40$ GeV.

$p_{\mathrm{T,jet}} = 110 < p_T < 160GeV$	Norm	α	β	γ
ATLAS data	4.96688	1.00499	0.01	9.15151
PYTHIA Log bin	5.3872	1.01577	0.519693	9.28972
PYTHIA Atlas bin	5.4077	1.01394	0.537594	9.15479

Table 3: Table showing example of the values after the fit procedure for each different fragmentation function data, according to equation 11 for $110 < p_{\mathrm{T,jet}} < 160$ GeV.

Splitting probability limits	Norm	ν	λ
Top limit	20	20	20
Low limit	0.01	0.15	0.01

Table 4: Table showing the limits applied to the parameters of the KKP parametrization. On the top row are the name of the parameters, the next row shows the higher limit this parameters can take, and the last row shows the lower limit for the parameters.

In order to solve the integral equation given in Eq. (5), a numerical method was used, since with the given forms, the equation does not have analytical solution. The method used was to fit the left hand side (the sum and the integral) of the equation with the right hand side (which was done using the fitted data with the error of the data). The solution is presented as the dashed line and is the probability splitting distribution.
In order to do so it is used the KKP fit obtained from the data as $F(z)$, and as $f(z)$ is used:

$$f(z) = N(1-z)^{\nu} e^{-z\lambda} \tag{12}$$

This shape is suggested from a previous study in our reserach group [54]. It includes only two parameters (λ and ν this one is different from the KKP form), where the exponential term $e^{-z\lambda}$ dominates at low z and $(1-z)^{\nu}$ dominates at high z. This shape, only having two parameters might be to stiff, but is able to get the general idea, as shown in [54]. The limits to the splitting probability are shown in Table 4. As previously, the limits are purely empirical.

Tables 5 and 6 shows examples of the values obtained on the fit. Making the limits more flexible lead to irregularities and clearly mistaken values. In some cases, without any limitation on the parameters, the fit gave parameters with negative values.

From the solution, which is a probability distribution by definition, the cascading model

$p_{\mathrm{T,jet}} = 25 < p_{\mathrm{T}} < 40 GeV$	Norm	ν	λ
ATLAS data	7.74873	0.150001	8.51991
PYTHIA Atlas bin	7.77324	0.15	8.37711
PYTHIA Log bin	7.97211	0.15	8.60002

Table 5: Table showing example of the values of the splitting probability, according to equation 12 for $25 < p_{\mathrm{T,jet}} < 40$ GeV.

$p_{\mathrm{T,jet}} = 110 < p_{\mathrm{T}} < 160 GeV$	Norm	ν	λ
ATLAS data	7.24494	0.15	8.48338
PYTHIA Atlas bin	7.30905	0.15	8.59116
PYTHIA Log bin	7.46366	0.15	8.79180

Table 6: Table showing example of the values of the splitting probability, according to equation 12 for $110 < p_{\mathrm{T,jet}} < 160$ GeV.

is implemented. At first is required the mean of the p_{T} trigger histogram, which is the mean of the p_{T} distribution in certain $p_{\mathrm{T,jet}}$. The next step is, taking this p_{T} value as the initial, to start splitting from it according to the probability distribution, until a limit, in this case 1 GeV. Each value obtained from the splitting is divided by the original energy value obtaining the z. The z values correspond to the red circles in Figs. 14, 15 and 16.
The results are presented with three different initial data. Figure 14 is the result of the previously described analysis using as the data to be fitted by the KKP parametrization the ATLAS data [32]. The cascade is able to reproduce the data reasonably, although is clear that is not equivalent. Also the data has large error bars, which lead us to do the PYTHIA simulation to improve the statistical errors. Figure 15 shows the same analysis taking PYTHIA simulated data. The error bars are clearly diminished with respect to Figure 14, but there is not significant difference in the shape, and in most cases the cascade done starting with ATLAS data shows a closer shape to the original data than the PYTHIA one. Finally, Figure 16 shows the results for logarithmic binning. The results become more similar to the ones obtained using ATLAS simulation.
In the appendixes is possible to find a more detailed analysis, for $25 < p_{\mathrm{T,jet}} < 500$ GeV energies, of the fitting and cascading performance. For higher energies the error bars of the PYTHIA data start to become larger, and above 260 GeV their fluctuations make them not so reliable for this analysis. The KKP fits agree decently with the data in most of the cases, showing always an underestimation for $z < 0.03$, which makes sense knowing the fit limits; and an overestimation for $z > 0.5$,which also makes sense, since in there are only a couple of points above that value. ATLAS data shows a stable pattern above 100 GeV for the cascading, and so does PYTHIA simulation in logarithmic binning. Nevertheless this latter data starts fluctuating above 260 GeV, as mentioned before. This same pattern is also can be seen in the PYTHIA simulation with ATLAS binning, but tends to exaggerate the values.

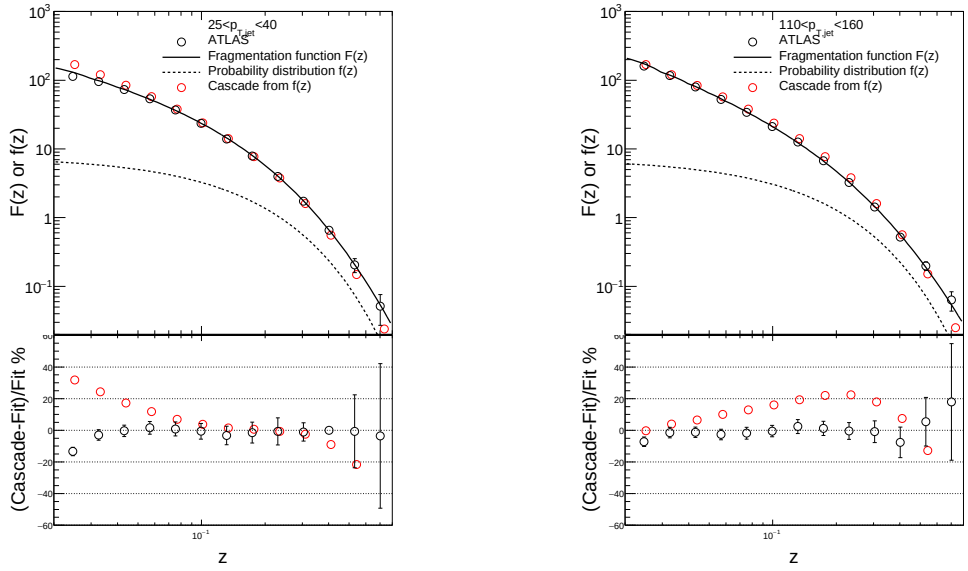

Figure 14: Fragmentation function obtained from ATLAS data [32] in $25 < p_{T,jet} < 40$ GeV (left) and $110 < p_{\mathrm{T,jet}} < 160$ GeV (right). Solid black line shows a fit to the fragmentation function in the form of Equation 11, and dotted black line a corresponding probability distribution solved from integral Equation 5. Open red circles are obtained trough cascade and should reproduce the solid line. The cascading circles have different position on the x-axis because the bin shift correction was not applied [55]. Lower panels show the ratio of ATLAS data and cascade result into the fit. Results in other jet transverse momentum bins are collected into Appendix B.

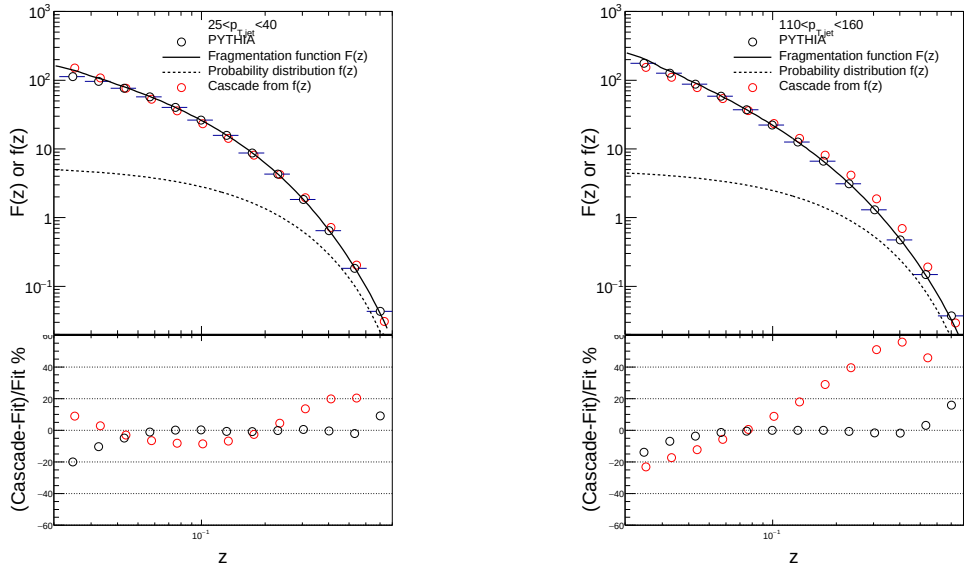

Figure 15: The same as in Figure 14, but using the PYTHIA data obtanined in my simulation, using the same binning as the ATLAS collaboration did. Results in other jet transverse momentum bins are collected into Appendix B.

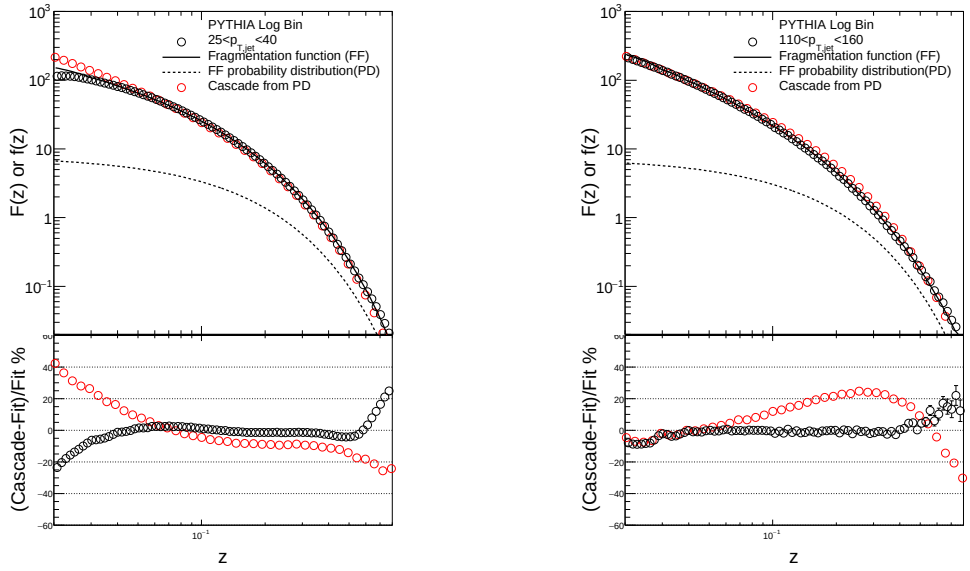

Figure 16: The same as in Figure 15, but using a logarithmic binning, using 50 bins in the region $0 < z < 1$. Results in other jet transverse momentum bins are collected into Appendix B.

7 Conclusions

The fragmentation functions from with the PYTHIA Monte Carlo event generator and the data from the ATLAS experiment in various jet energy ranges were used to study a cascade model proposed by Richard Feymann and Richard Field. Finally the analysis of the results lead to the following conclusions: PYTHIA8 8.212 is able to estimate the measured fragmentation function from the ATLAS experiment within a 20% for most of the $p_{\mathrm{T,jet}}$ energies. These discrepancies are reached in regions around $z = 0.1$ (+20%) and $z > 0.7$ (-20%) for lower $p_{\mathrm{T,jet}}$ energies; for the higher momentum jets, PYTHIA tends to describe the data better but still overestimates (+10%) the data at the lower z, good description in the intermediate z ranges.

The PYTHIA simulation or real ATLAS data are fitted with the KKP parametrization. For most of the data sets, the fit tends to underestimate the data (-20%) at $0 < z < 0.05$. This might be explained by the fact that for convergence, the fit is made in the range $0.03 < z < 0.99$. Then at $z > 0.6$ the fit starts to overestimate the data. The fit performance is better when using logarithmic binning. Nevertheless, for higher energies in high z this binning form shows more fluctuations. With ATLAS data the fit stays mostly within the error bars.

After solving the Integral equation (5) using the fit, the splitting probability is obtained. The cascading model is able to reproduce the data within a 20% in most of the $p_{\mathrm{T,jet}}$ energy ranges. When the $p_{\mathrm{T,jet}}$ increases, the cascade simulation starts to deviate more from the data. For $z = 0$ usually presents an underestimation (-20%), then starts to grow linearly (with logarithmic scale on the x-axis) up to $z = 0.3$ giving an overestimation around +50%, crossing with the data around $z = 0.06$. Then starts again to decrease to match the data for $z > 0.7$. The cause of this discrepancy might be the functional form chosen for the splitting probability on equation 12. Using a more flexible form with more parameters might improve the results, but that would difficult the solution of the integral equation 5.

8 Appendix A: Z-distribution figures for different jet energies.

In this Appendix, the fragmentation function comparison between ATLAS and PYTHIA simulation data is shown for all the $p_{T,jet}$ ranges available (from 25 to 500 GeV).

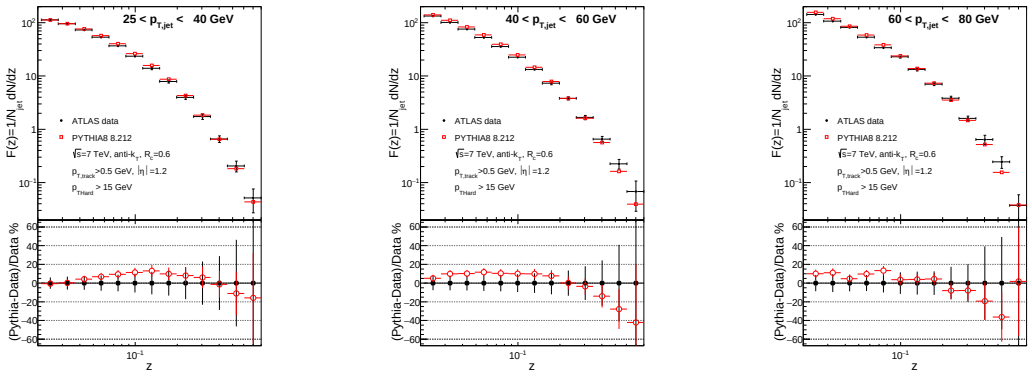

Figure 17: Z-distribution for PYTHIA simulation compared to ATLAS data for $25 < p_{T,bin} < 40$, $40 < p_{T,bin} < 60$ and $60 < p_{T,bin} < 80$.

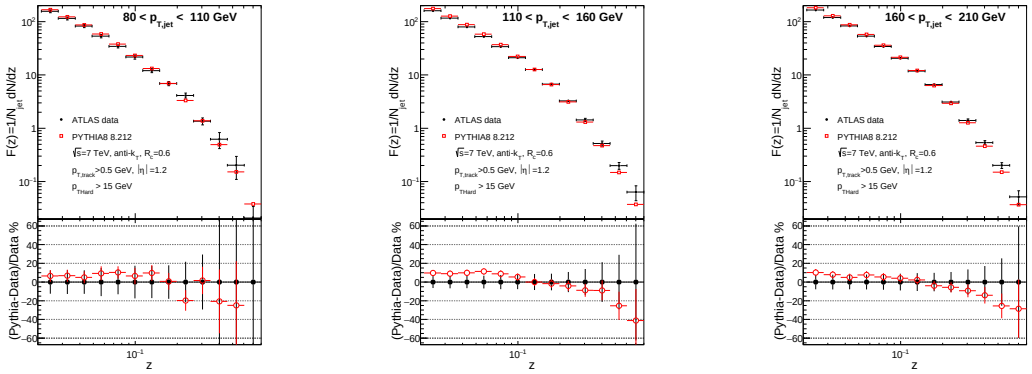

Figure 18: Z-distribution for PYTHIA simulation compared to ATLAS data for $80 < p_{T,bin} < 110$, $110 < p_{T,bin} < 160$ and $160 < p_{T,bin} < 210$

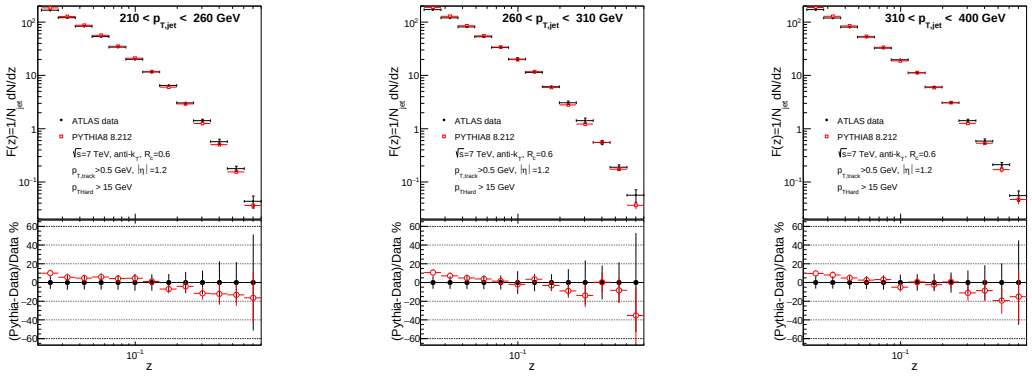

Figure 19: Z-distribution for PYTHIA simulation compared to ATLAS data for $210 < p_{T,bin} < 260$, $260 < p_{T,bin} < 310$ and $310 < p_{T,bin} < 400$

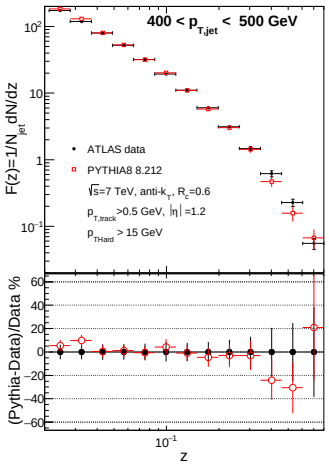

Figure 20: Z-distribution for PYTHIA simulation compared to ATLAS data for $400 < p_{T,bin} < 500$

9 Appendix B: Feynman analysis figures and tables for different jet energies.

In this Appendix, the Feynman cascading model is implemented taking as the true fragmentation function ATLAS data, PYTHIA simulation and PYTHIA simulation with logarithmic binning. For each energy there is also a table with the deviation of the KKP functional form fit and the cascade simulation. For each initial data (ATLAS data, PYTHIA simulation and PYTHIA simulation with logarithmic binning) is given the highest deviation of the data for high z and low z in percentage according to the ratio panels. The arrows next to the values show if the deviation of the data is above or below the KKP fit

9.1 Jet Energy: $p_{T,jet} = 25 < p_T < 40$ GeV

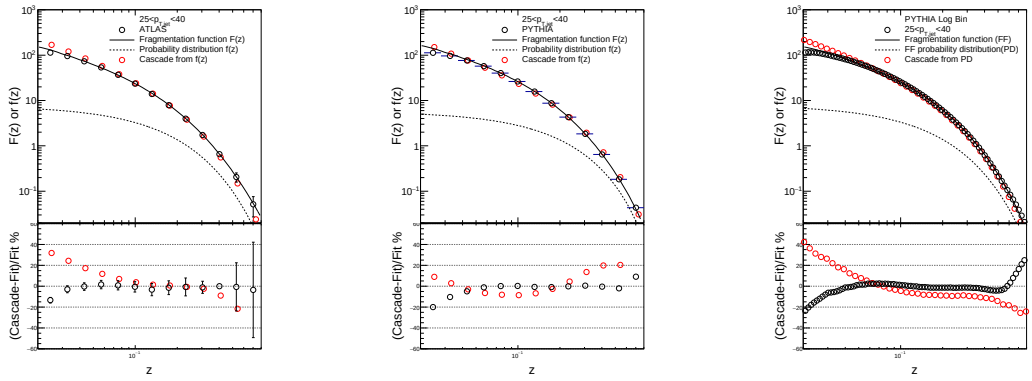

Figure 21

$p_{T,jet} = 25 < p_T < 40 GeV$	Original data		Feynman cascade	
	Low z	High z	Low z	High z
ATLAS data	15% ↓	5% ↓	35% ↑	20% ↓
PYTHIA Atlas bin	20% ↓	10% ↑	10% ↑	20% ↑
PYTHIA Log bin	20% ↓	25% ↑	45% ↑	25% ↓

9.2 Jet Energy: $p_{T,jet} = 40 < p_T < 60$ GeV

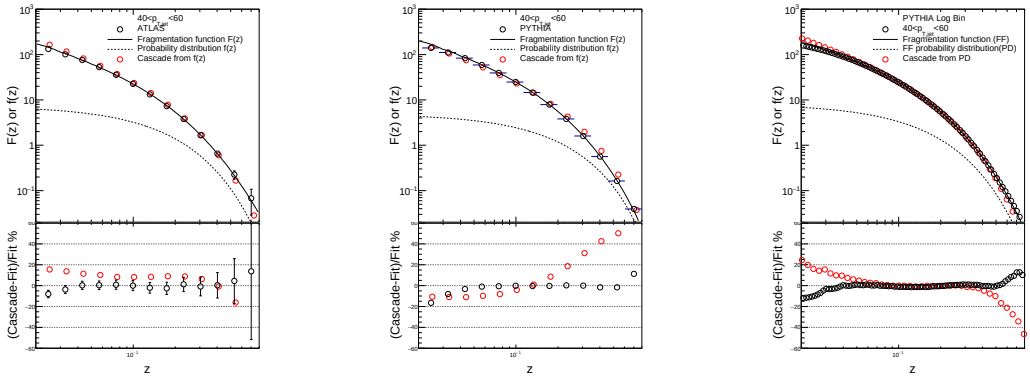

$p_{T,jet} = 40 < p_T < 60 GeV$	Original data		Feynman cascade	
	Low z	High z	Low z	High z
ATLAS data	10% ↓	20% ↑	20% ↑	20% ↓
PYTHIA Atlas bin	20% ↓	20% ↑	20% ↓	60% ↑
PYTHIA Log bin	10% ↓	10% ↑	35% ↑	diverges ↓

Figure 22

9.3 Jet Energy: $p_{T,jet} = 60 < p_T < 80$ GeV

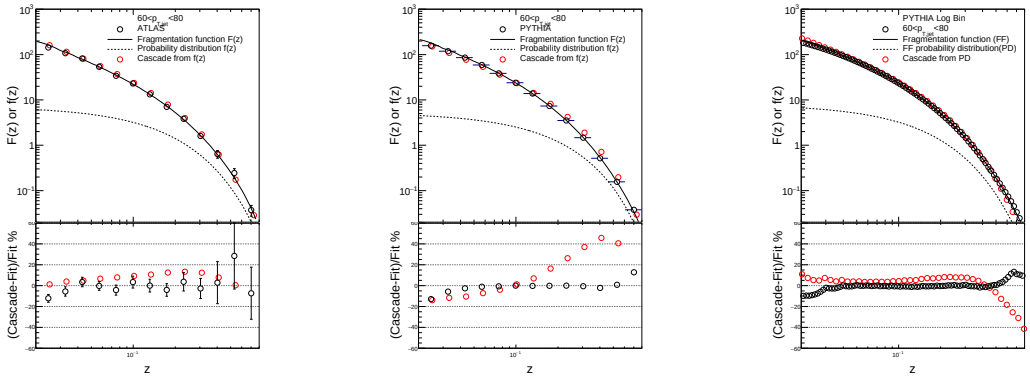

Figure 23

$p_{T,jet} = 60 < p_T < 80 GeV$	Original data		Feynman cascade	
	Low z	High z	Low z	High z
ATLAS data	15% ↓	30% ↑	5% ↑	15% ↑
PYTHIA Atlas bin	15% ↓	15% ↑	15% ↓	45% ↓
PYTHIA Log bin	10% ↓	10% ↑	20% ↑	diverges ↓

9.4 Jet Energy: $p_{T,jet} = 80 < p_T < 110$ GeV

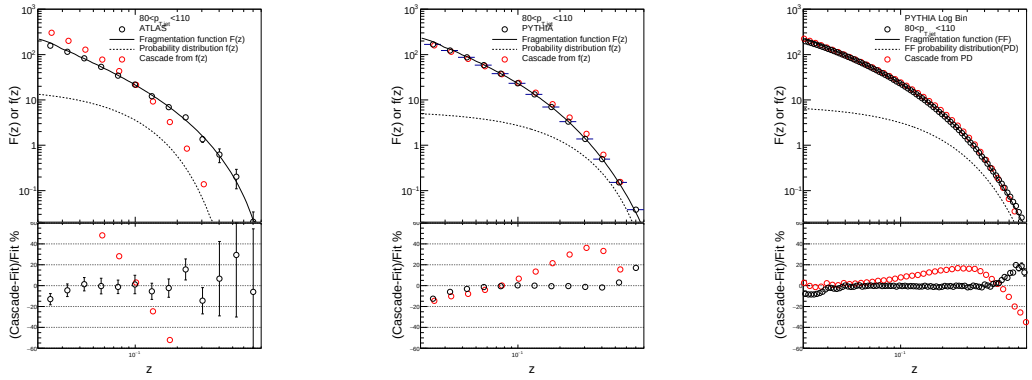

Figure 24: In this figure, on the ATLAS data figure the cascading process diverges completely. The solution of the integral equation might be wrong for this particular case owe to parameter limitation. It is possible that the probability distribution.

$p_{T,jet} = 80 < p_T < 110 GeV$	Original data		Feynman cascade	
	Low z	High z	Low z	High z
ATLAS data	15% ↓	30% ↑	-	-
PYTHIA Atlas bin	15% ↓	20% ↑	15% ↓	40% ↓
PYTHIA Log bin	10% ↓	20% ↑	10% ↑	diverges ↓

9.5 Jet Energy: $p_{T,jet} = 110 < p_T < 160$ GeV

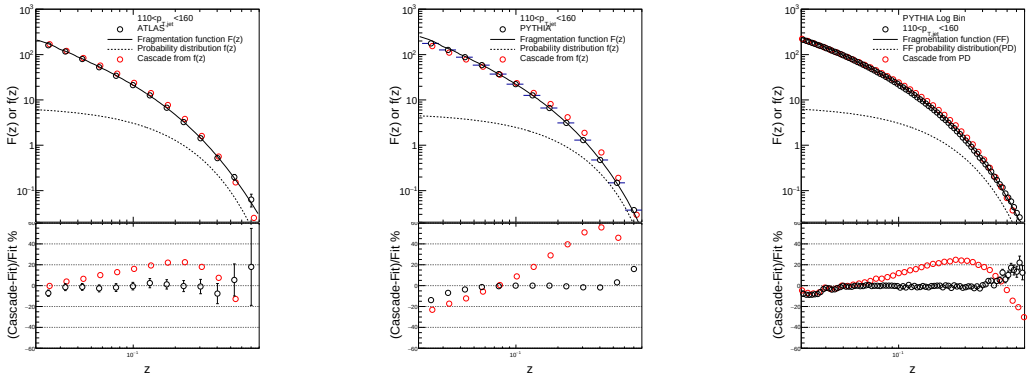

Figure 25

$p_{T,jet} = 110 < p_T < 160 GeV$	Original data		Feynman cascade	
	Low z	High z	Low z	High z
ATLAS data	5% ↓	20% ↑	10% ↓	15% ↓
PYTHIA Atlas bin	15% ↓	20% ↑	20% ↓	60% ↓
PYTHIA Log bin	10% ↓	20% ↑	10% ↑	diverges ↓

9.6 Jet Energy: $p_{T,jet} = 160 < p_T < 210$ GeV

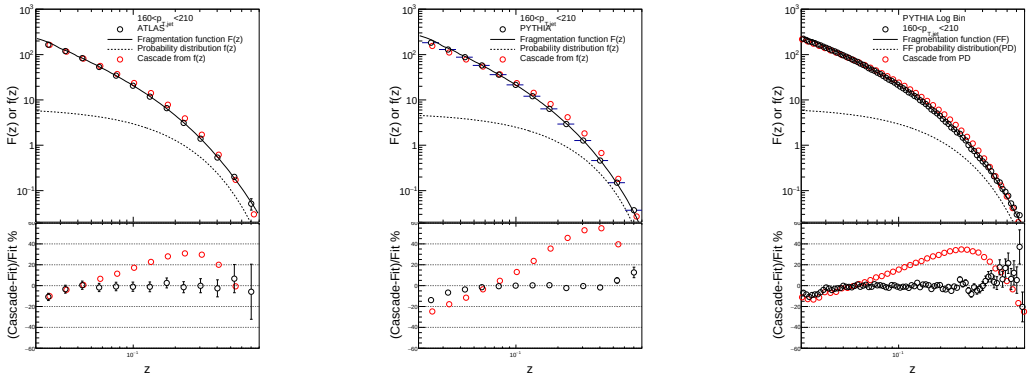

Figure 26

$p_{T,jet} = 160 < p_T < 210 GeV$	Original data		Feynman cascade	
	Low z	High z	Low z	High z
ATLAS data	10% ↓	5% ↓	10% ↓	30% ↓
PYTHIA Atlas bin	15% ↓	15% ↑	25% ↓	55% ↓
PYTHIA Log bin	10% ↓	20% ↑	5% ↑	diverges ↓

9.7 Jet Energy: $p_{T,jet} = 210 < p_T < 260$ GeV

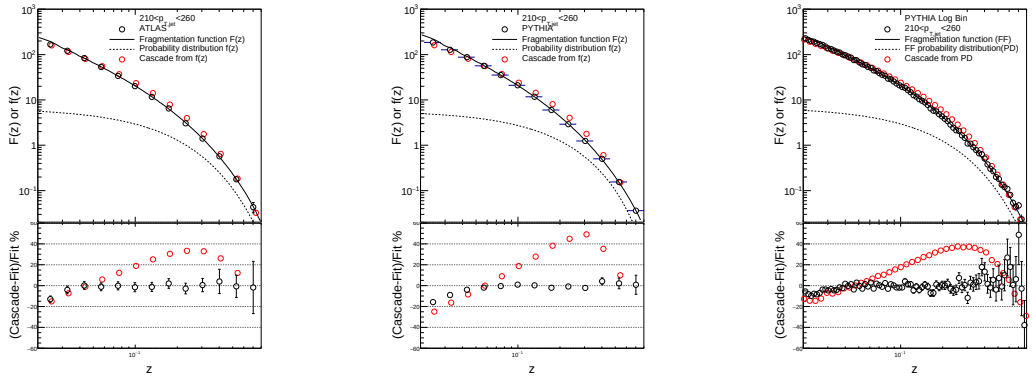

Figure 27

$p_{T,jet} = 210 < p_T < 260 GeV$	Original data		Feynman cascade	
	Low z	High z	Low z	High z
ATLAS data	15% ↓	5% ↑	20% ↓	35% ↑
PYTHIA Atlas bin	15% ↓	5% ↑	25% ↓	50% ↓
PYTHIA Log bin	5% ↓	lack of statistics	5% ↑	diverges ↓

9.8 Jet Energy: $p_{T,jet} = 260 < p_T < 310$ GeV

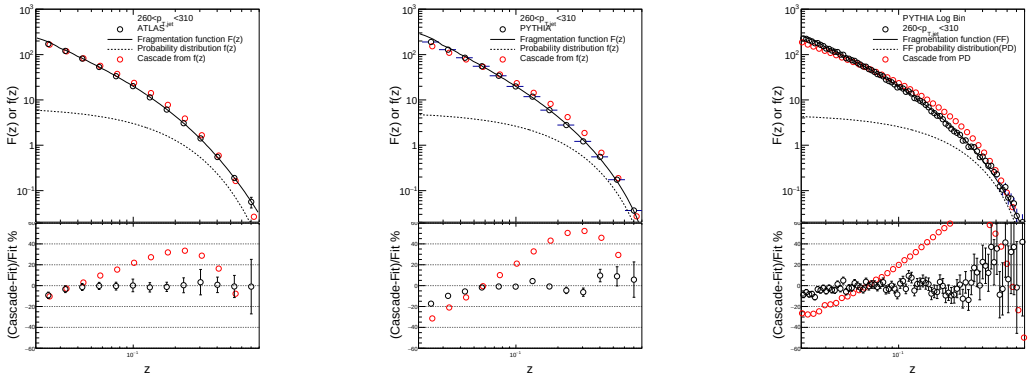

Figure 28

$p_{T,jet} = 260 < p_T < 310 GeV$	Original data		Feynman cascade	
	Low z	High z	Low z	High z
ATLAS data	10% ↓	5% ↑	10% ↓	35% ↑
PYTHIA Atlas bin	20% ↓	15% ↑	35% ↓	55% ↓
PYTHIA Log bin	10% ↓	lack of statistics	10% ↑	diverges ↓

9.9 Jet Energy: $p_{T,jet} = 310 < p_T < 400$ GeV

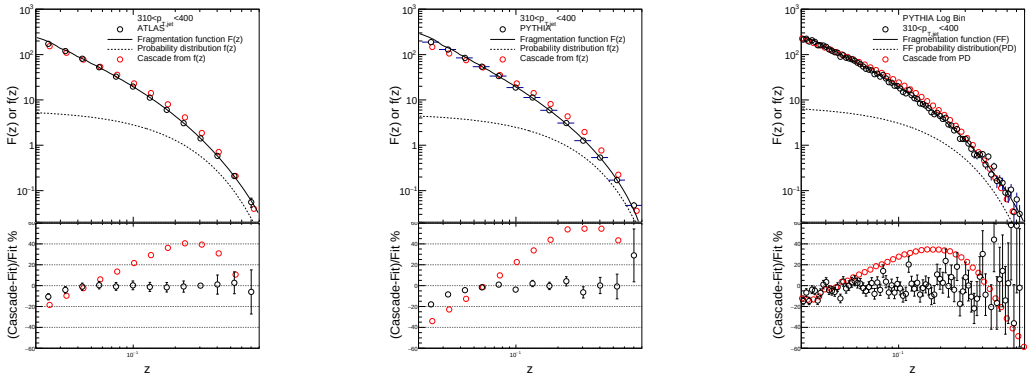

Figure 29

$p_{T,jet} = 310 < p_T < 400GeV$	Original data		Feynman cascade	
	Low z	High z	Low z	High z
ATLAS data	10% ↓	5% ↑	20% ↓	40% ↑
PYTHIA Atlas bin	20% ↓	30% ↑	35% ↓	50% ↓
PYTHIA Log bin	10% ↓	lack of statistics	10% ↑	diverges ↓

9.10 Jet Energy: $p_{T,jet} = 400 < p_T < 500$ GeV

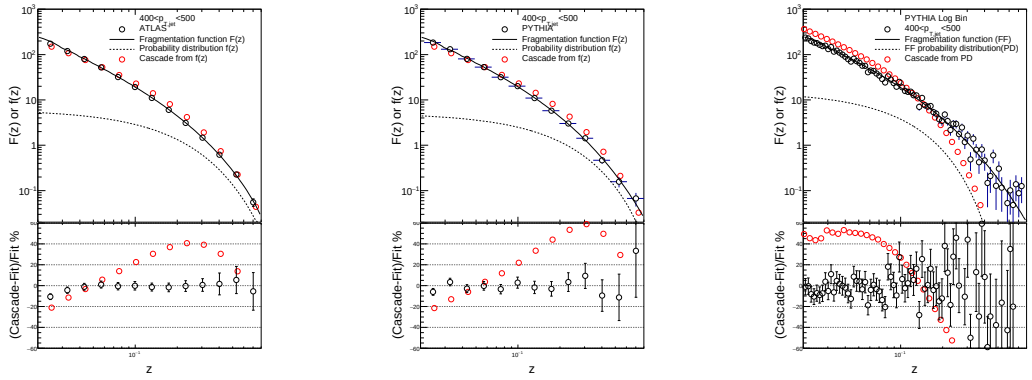

Figure 30

$p_{T,jet} = 400 < p_T < 500 GeV$	Original data		Feynman cascade	
	Low z	High z	Low z	High z
ATLAS data	10% ↓	5% ↑	20% ↓	40% ↑
PYTHIA Atlas bin	5% ↓	35% ↑	20% ↓	50% ↓
PYTHIA Log bin	lack of statistics	lack of statistics	-	-

References

[1] Murray Gell-Mann. Symmetries of baryons and mesons. *Phys. Rev.*, 125:1067–1084, Feb 1962.

[2] R. Brandelik et al. Evidence for planar events in e+e annihilation at high energies. *Physics Letters B*, 86(2):243 – 249, 1979.

[3] G. Zweig. An SU(3) model for strong interaction symmetry and its breaking. Version 2. In D.B. Lichtenberg and Simon Peter Rosen, editors, *DEVELOPMENTS IN THE QUARK THEORY OF HADRONS. VOL. 1. 1964 - 1978*, pages 22–101. 1964.

[4] M. Gell-Mann. A schematic model of baryons and mesons. *Physics Letters*, 8(3):214 – 215, 1964.

[5] B.J. Bjorken and S.L. Glashow. Elementary particles and su(4). *Physics Letters*, 11(3):255 – 257, 1964.

[6] Makoto Kobayashi and Toshihide Maskawa. Cp-violation in the renormalizable theory of weak interaction. *Progress of Theoretical Physics*, 49(2):652–657, 1973.

[7] E. D. Bloom, D. H. Coward, H. DeStaebler, J. Drees, G. Miller, L. W. Mo, R. E. Taylor, M. Breidenbach, J. I. Friedman, G. C. Hartmann, and H. W. Kendall. High-energy inelastic $e - p$ scattering at 6° and 10°. *Phys. Rev. Lett.*, 23:930–934, Oct 1969.

[8] M. Breidenbach, J. I. Friedman, H. W. Kendall, E. D. Bloom, D. H. Coward, H. DeStaebler, J. Drees, L. W. Mo, and R. E. Taylor. Observed behavior of highly inelastic electron-proton scattering. *Phys. Rev. Lett.*, 23:935–939, Oct 1969.

[9] J. E. Augustin, A. M. Boyarski, M. Breidenbach, F. Bulos, J. T. Dakin, G. J. Feldman, G. E. Fischer, D. Fryberger, G. Hanson, B. Jean-Marie, R. R. Larsen, V. Lüth, H. L. Lynch, D. Lyon, C. C. Morehouse, J. M. Paterson, M. L. Perl, B. Richter,

P. Rapidis, R. F. Schwitters, W. M. Tanenbaum, F. Vannucci, G. S. Abrams, D. Briggs, W. Chinowsky, C. E. Friedberg, G. Goldhaber, R. J. Hollebeek, J. A. Kadyk, B. Lulu, F. Pierre, G. H. Trilling, J. S. Whitaker, J. Wiss, and J. E. Zipse. Discovery of a narrow resonance in e^+e^- annihilation. *Phys. Rev. Lett.*, 33:1406–1408, Dec 1974.

[10] S. W. Herb, D. C. Hom, L. M. Lederman, J. C. Sens, H. D. Snyder, J. K. Yoh, J. A. Appel, B. C. Brown, C. N. Brown, W. R. Innes, K. Ueno, T. Yamanouchi, A. S. Ito, H. Jöstlein, D. M. Kaplan, and R. D. Kephart. Observation of a dimuon resonance at 9.5 gev in 400-gev proton-nucleus collisions. *Phys. Rev. Lett.*, 39:252–255, Aug 1977.

[11] F. et al Abe. Observation of top quark production in $\overline{p}p$ collisions with the collider detector at fermilab. *Phys. Rev. Lett.*, 74:2626–2631, Apr 1995.

[12] O. W. Greenberg. Spin and unitary-spin independence in a paraquark model of baryons and mesons. *Phys. Rev. Lett.*, 13:598–602, Nov 1964.

[13] D. Griffiths. *Introduciton to Elementary Particles*. John Wiley & Sons, 1987.

[14] B.R. Martin and G. Shaw. *Particle Physics*. John Wiley & Sons, 2008.

[15] Stanley J. Brodsky. High energy photon-photon collisions at a linear collider. *Int. J. Mod. Phys.*, A20:7306–7332, 2005.

[16] Richard M. Dummit, David S.; Foote. *Abstract Algebra*. John Wiley & Sons, 2004.

[17] David J. Gross and Frank Wilczek. Ultraviolet behavior of non-abelian gauge theories. *Phys. Rev. Lett.*, 30:1343–1346, Jun 1973.

[18] Siegfried Bethke. Experimental tests of asymptotic freedom. *Prog. Part. Nucl. Phys.*, 58:351–386, 2007.

[19] John C. Collins, Davison E. Soper, and George F. Sterman. Factorization of Hard Processes in QCD. *Adv. Ser. Direct. High Energy Phys.*, 5:1–91, 1989.

[20] R. Oerter. *The Theory of Almost Everything: The Standard Model, the Unsung Triumph of Modern Physics*. Penguin Group, 2006.

[21] David d'Enterria, Kari J. Eskola, Ilkka Helenius, and Hannu Paukkunen. LHC data challenges the contemporary parton-to-hadron fragmentation functions. *PoS*, DIS2014:148, 2014.

[22] J. F. Owens. Large Momentum Transfer Production of Direct Photons, Jets, and Particles. *Rev. Mod. Phys.*, 59:465, 1987.

[23] R. K. Adair. *The Great Design: Particles, Fields, and Creation*. Oxford University Press, 1989.

[24] Ringaile Placakyte. Parton Distribution Functions. In *Proceedings, 31st International Conference on Physics in collisions (PIC 2011): Vancouver, Canada, August 28-September 1, 2011*, 2011.

[25] John M. Campbell, J. W. Huston, and W. J. Stirling. Hard Interactions of Quarks and Gluons: A Primer for LHC Physics. *Rept. Prog. Phys.*, 70:89, 2007.

[26] Ralf Seidl. Fragmentation function measurements. *PoS*, Hadron2013:026, 2013.

[27] J. F. Owens. Large-momentum-transfer production of direct photons, jets, and particles. *Rev. Mod. Phys.*, 59:465–503, Apr 1987.

[28] Francois Arleo, Redamy Perez Ramos, and Bruno Machet. Hadronic single inclusive k-perpendicular distributions inside one jet beyond MLLA. *Phys. Rev. Lett.*, 100:052002, 2008.

[29] Redamy Perez-Ramos, Francois Arleo, and Bruno Machet. Next-to-MLLA corrections to single inclusive k^- perp-distributions and 2-particle correlations in a jet. *Phys. Rev.*, D78:014019, 2008.

[30] G. Aad et al. Measurement of inclusive jet and dijet cross sections in proton-proton collisions at 7 TeV centre-of-mass energy with the ATLAS detector. *Eur. Phys. J.*, C71:1512, 2011.

[31] R. D. Field and R. P. Feynman. A Parametrization of the Properties of Quark Jets. *Nucl. Phys.*, B136:1, 1978.

[32] Georges Aad et al. Measurement of the jet fragmentation function and transverse profile in proton-proton collisions at a center-of-mass energy of 7 TeV with the ATLAS detector. *Eur. Phys. J.*, C71:1795, 2011.

[33] A. D. Halzen, F. ; Martin. *Quarks and Leptons: An Introductory Course in Modern Particle Physics*. John Wiley & Sons, 1984.

[34] G. Aad et al. The ATLAS Experiment at the CERN Large Hadron Collider. *JINST*, 3:S08003, 2008.

[35] The ALICE Collaboration et al. The alice experiment at the cern lhc. *Journal of Instrumentation*, 3(08):S08002, 2008.

[36] S. Chatrchyan et al. The CMS experiment at the CERN LHC. *JINST*, 3:S08004, 2008.

[37] A. Augusto Alves, Jr. et al. The LHCb Detector at the LHC. *JINST*, 3:S08005, 2008.

[38] Torbjorn Sjostrand, Stephen Mrenna, and Peter Z. Skands. A Brief Introduction to PYTHIA 8.1. *Comput. Phys. Commun.*, 178:852–867, 2008.

[39] G. Corcella, I. G. Knowles, G. Marchesini, S. Moretti, K. Odagiri, P. Richardson, M. H. Seymour, and B. R. Webber. HERWIG 6: An Event generator for hadron emission reactions with interfering gluons (including supersymmetric processes). *JHEP*, 01:010, 2001.

[40] Ahmed Ali and Gustav Kramer. Jets and QCD: A Historical Review of the Discovery of the Quark and Gluon Jets and its Impact on QCD. *Eur. Phys. J.*, H36:245–326, 2011.

[41] Richard P. Feynman. *The Behavior of Hadron Collisions at Extreme Energies*, pages 289–304. Springer Netherlands, Dordrecht, 1988.

[42] A.H. Mueller. Multiplicity and hadron distributions in qcd jets. *Nuclear Physics B*, 213(1):85 – 108, 1983.

[43] R. Barger, V. ; Phillips. *Collider Physics*. Addison-Wesley, 1997.

[44] Pavel Weber. *ATLAS Calorimetry: Trigger, Simulation and Jet Calibration*. PhD thesis, Kirchhoff Institut Fr Physik, 2008.

[45] Rick D. Field. The Underlying event in hard scattering processes. *eConf*, C010630:P501, 2001.

[46] Gerald C. Blazey et al. Run II jet physics. In *QCD and weak boson physics in Run II. Proceedings, Batavia, USA, March 4-6, June 3-4, November 4-6, 1999*, pages 47–77, 2000.

[47] Stephen D. Ellis and Davison E. Soper. Successive combination jet algorithm for hadron collisions. *Phys. Rev.*, D48:3160–3166, 1993.

[48] Yuri L. Dokshitzer, G. D. Leder, S. Moretti, and B. R. Webber. Better jet clustering algorithms. *JHEP*, 08:001, 1997.

[49] Matteo Cacciari, Gavin P. Salam, and Gregory Soyez. The Anti-k(t) jet clustering algorithm. *JHEP*, 04:063, 2008.

[50] Matteo Cacciari, Gavin P. Salam, and Gregory Soyez. FastJet User Manual. *Eur. Phys. J.*, C72:1896, 2012.

[51] Esko Pohjoisaho. Pythia study of isolation cuts in x_T distributions. Research Report, August 2012, not published.

[52] K. A. Olive et al. Review of Particle Physics. *Chin. Phys.*, C38:090001, 2014.

[53] B.A. Kniehl, G. Kramer, and B. Ptter. Fragmentation functions for pions, kaons, and protons at next-to-leading order. *Nuclear Physics B*, 582(1):514 – 536, 2000.

[54] Petja Paakkinen. Monte carlo simulation of dihadron correlations at midrapidity in p+p collisions. Research Report, November 2014, not published.

[55] G.D. Lafferty and T.R. Wyatt. Where to stick your data points: The treatment of measurements within wide bins. *Nuclear Instruments and Methods in Physics Research Section A: Accelerators, Spectrometers, Detectors and Associated Equipment*, 355(2):541 – 547, 1995.